Research Letter **DOI:** 10.15541/jim20250103

Facile Fabrication of Ceramic-resin Coatings on C/CA Composites for Oxidation Protection at Medium Temperatures

TIAN Hongwang[1,2], LUO Longfei[3], HU Chenglong[1], YAN Meng[1], PANG Shengyang[1], LI Jian[1], TANG Sufang[1]

(1. Institute of Metal Research, Chinese Academy of Sciences, Shenyang 110016, China; 2. School of Materials Science and Engineering, University of Science and Technology of China, Shenyang 110016, China; 3. Xi'an Aerospace Composites Research Institute, Xi'an 710025, China)

Abstract: Carbon fiber-reinforced carbon aerogel (C/CA) composites are one of the most promising candidates for applications requiring both thermal insulation and load bearing capabilities. The preparation of anti-oxidation coatings on C/CA to address its susceptibility to oxidation is a feasible approach to promote its application in oxidative environments. However, the currently reported coatings on C/CA mainly focus on improving the ablation performance and coating preparation process typically necessitating high-temperature heat treatment. This procedure can increase its thermal conductivity and reduce its thermal insulation ability. In this study, a series of ceramic-resin coatings were fabricated on C/CA through a simple slurry brushing-drying approach at room temperature. The effects of phenolic resin content on the coating structure, residual stress, thermal shock, and oxidation behaviors were investigated. Due to the adhesive properties and curing-induced shrinkage, the PR-7.5 coating (containing 7.5% (in mass) phenolic resin in the slurry) exhibits bonding strength close to fracture strength of the substrate and residual compressive stress of 0.853 GPa, which is beneficial for resisting thermal shock cracking. However, excessive resin content (PR-10.0 containing 10.0% (in mass) phenolic resin in the slurry) induces tensile stress due to uneven curing shrinkage, thereby leading to thermal shock cracking. Meanwhile, oxidation tests reveal significantly reduced weight losses for PR-7.5 (17.46% at 800 ℃/100 min, 8.15% at 1000 ℃/120 min, 3.15% at 1200 ℃/120 min) *versus* uncoated C/CA's 44.60% loss at 800 ℃/20 min. This work provides a brand-new and simple approach to improving the anti-oxidation performance of C/CA and expands its application in mild oxidative environments.

Key words: C/CA composite; coating; oxidation; residual stress; interfacial bonding

Carbon aerogels (CAs) are highly porous materials characterized by a unique skeleton structure comprising three-dimensionally overlapped nanoparticles and interconnected nanopores, which endows them with low bulk density, large specific surface area and low thermal conductivity compared to other carbon materials[1]. Comparatively, carbon fiber-reinforced carbon aerogel (C/CA) composites, prepared by carbonization of organic fiber reinforced organic aerogel, exhibit low density, low thermal conductivity, and high thermal stability up to 2000 ℃, along with good mechanical properties that facilitate the manufacture of large bulks. Notably, these composites present a specific compressive strength of 160 $MPa \cdot g^{-1} \cdot cm^3$ and a fracture energy of 354 J/m^2, which are the highest values among the reported various aerogel materials[2]. Resultantly, C/CA composites demonstrate tremendous potential in the applications requiring both thermal insulation and load bearing. However, the high oxygen sensitivity of C/CA significantly restricts their application in high-temperature oxidizing environments, as evidenced by a lower apparent activation energy of 50.80 kJ/mol compared to the traditional carbon materials, along with a reduced initial oxidation temperature of 350 ℃[3]. In consequence,

Received date: 2025-03-11; **Revised date:** 2025-05-19; **Published online:** 2025-05-22
Foundation item: National Natural Science Foundation of China (52272075, 52472053); Research Fund of Youth Innovation Promotion Association of CAS, China (2021190); Defense Industrial Technology Development Program (JCKY2021130B007)
Biography: TIAN Hongwang (1999–), male, Master candidate. E-mail: hwtian22s@imr.ac.cn
田洪旺(1999–), 男, 硕士研究生. E-mail: hwtian22s@imr.ac.cn
Corresponding author: HU Chenglong, professor. E-mail: clhu10s@imr.ac.cn
胡成龙, 研究员. E-mail: clhu10s@imr.ac.cn

it becomes pivotal to improve the oxidation resistance of C/CA in order to broaden their applicability and prolong their service life.

Applying a ceramic coating on C/CA is a promising strategy for improving their long-term service abilities in oxidizing environments[4-5]. However, reports on oxidation-resistant coatings for C/CA and other porous carbon materials remain sparse. Yan *et al.*[6-7] prepared SiC monolayer, SiC bilayer and SiC/ZrB_2-SiC bilayer coatings on C/CA composites successively through gas-solid reaction between Si and CA matrix at high temperatures (1300–1400 ℃). Benefiting from the dense surface and gradient structure, these coatings could withstand oxyacetylene ablation at 1650–1900 ℃ for durations of 600 s to 900 s. Xu *et al.*[8] prepared HfB_2-$MoSi_2$ coatings on carbon-bonded carbon fiber (CBCF) *via* thermal spraying, resulting in a low mass ablation rate of 5.8×10^{-4} $g\cdot cm^{-2}\cdot s^{-1}$ after exposure to ablation at 1500–2200 ℃ for 480 s. Through a rapid sintering process in a micro-oxygen environment, Li *et al.*[9] and Xu *et al.*[10] applied ceramic-glass coatings on C/CA-SiCO and CBCF/ZrB_2, respectively, achieving good ablation resistance at 1600 ℃ for 200–800 s. Nevertheless, the current studies on oxidation-resistant coatings for porous carbon materials mainly focus on improving the ablation properties for brief periods (tens to hundreds of seconds), with limited reports about the antioxidant properties at medium temperatures (*e.g.*, 800–1200 ℃) over extended durations. In addition, the current fabrication methods for anti-oxidant coatings typically necessitate high-temperature heat treatment, which can adversely affect the increase in solid thermal conductivity of C/CA due to the rearrangement of carbon atoms[11]. Therefore, further studies are warranted to develop ceramic coatings at low or even room temperature for C/CA to maintain its low thermal conductivity and achieve long-duration oxidation resistance. To ensure the continuous and stable existence of the oxide film, this study adopted a multi-ceramic composite strategy. By taking advantage of the differences in the initial oxidation temperatures of silicon and boron-based ceramics, a hybrid ceramic system with different initial oxidation temperatures was constructed. Oxidation reactions occurred sequentially in different ceramics at 800–1200 ℃, thus establishing a stepped synergistic protective effect.

Here, we report a ceramic-resin coating on C/CA utilizing a simple slurry brushing-drying process at room temperature. Effects of phenolic resin content in the coated C/CA on the coating structure, interfacial bonding, residual stress, thermal shock and oxidation behavior were investigated.

1 Experimental

1.1 Coating preparation

C/CA composites with a density of 0.6 $g\cdot cm^{-3}$ were prepared using phenolic resin and ethylene glycol, following the method described in our previous studies[12]. Subsequently, they were cut into small pieces with dimensions of 15 mm×15 mm×10 mm for testing. After being polished, the samples were ultrasonically cleaned in ethanol and dried at 100 ℃ for 2 h.

The coating preparation process consists of three steps. Firstly, 12.5%–22.5% (in mass) SiC (1 μm), 47.5%–57.5% (in mass) B_4C (1 μm), 2%–8% (in mass) SiO_2 (50 nm), 3%–7% (in mass) B_2O_3 (1 μm), 7.5%–12.5% (in mass) SiB_6 (1 μm), and 5%–9% (in mass) $ZrSi_2$ (1 μm) powders were mixed by ball milling to form the solid phase of the slurries. The aforementioned ceramic mixture accounts for 20% (in mass) of the total slurry mass, while polyvinyl butyral (PVB) resin constitutes 10% (in mass) of the total slurry mass. The combined mass of phenolic resin and ethanol makes up the remaining 70% (in mass) of the total slurry mass. Four distinct coating groups were prepared by adjusting the mass percentage of phenolic resin in the slurry (0, 5.0%, 7.5%, and 10.0% (in mass), denoted as PR-0, PR-5.0, PR-7.5, and PR-10.0, respectively). Secondly, the slurries were applied on the C/CA substrates using a brushing method. Thirdly, the C/CA coated with slurries was dried at room temperature to facilitate the formation of coatings containing ceramic powders and resin. Fig. S1 shows the macrophotograph of the coated C/CA panel.

1.2 Testing methods for thermal shock and oxidation resistance

Thermal shock resistance of the coatings with different phenolic resin contents was tested in static air using a muffle furnace. Specifically, the samples were subjected to a temperature of 1200 ℃ for a duration of 5 min. Then, they were taken out and cooled to room temperature in ambient air. Following the cooling process, the samples were weighed and reintroduced into the furnace for the subsequent thermal shock cycle. The oxidation resistance of the coating was assessed through an isothermal oxidation test in static air. The muffle furnace was heated to the designated temperatures (800, 1000, and 1200 ℃). The weight loss of the samples was measured every 20 min. The cumulative oxidation time at 800, 1000, and 1200 ℃ were 100, 120, and 120 min, respectively.

1.3 Microstructure and composition characterization

The microstructures of the samples before and after oxidation were observed using a scanning electron microscope (SEM, Thermo Scientific, Verios G4 UC), equipped with energy-dispersive X-ray spectroscopy (EDS). The composition of the coatings was determined by X-ray diffraction (XRD). The oxidation behaviors of the ceramic powders used for the coating preparation were also measured using a thermogravimetric analyzer (NETZSCH STA 449 F5).

2 Results and discussion

2.1 Microstructure and composition

Fig. 1 displays the surface and cross-section morphologies of ceramic-resin coatings with varying phenolic resin contents. Evidently, the coatings become more compact and thicker as the phenolic resin content rises. The phenolic resin-free coating (PR-0) shown in Fig. 1(a) has a fragmented appearance with numerous micron-sized inter-particle pores. Upon 5.0% addition of phenolic resin, the as-prepared PR-5.0 displays a reduction in pore size, although the surface remains porous (Fig. 1(b)). As the content increases to 7.5%, the resin fills the inter-particle pores, resulting in a denser surface for PR-7.5 (Fig. 1(c)). The surface of PR-10.0 is smooth and compact due to excessive phenolic resin covering the surface (Fig. 1(d)). This observation is further supported by the gradually intensified broad halo in the XRD patterns shown in Fig. S2, confirming the presence of amorphous resin in PR-10.0. The insets in Fig. 1 indicate the thicknesses of PR-0, PR-5.0, PR-7.5 and PR-10.0 to be 76.6, 135.4, 173.6 and 254.1 μm, respectively.

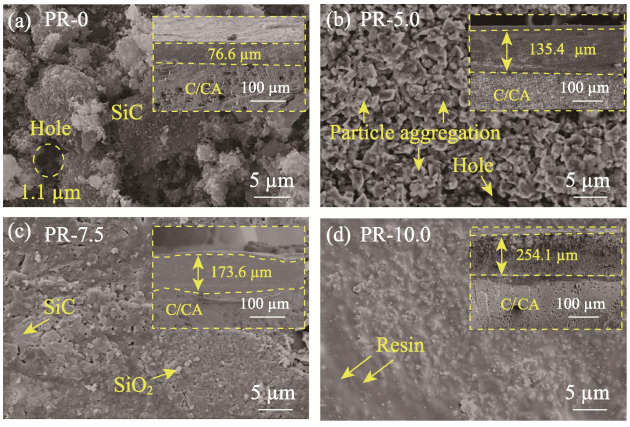

Fig. 1 Surface and cross-sectional morphologies of (a) PR-0, (b) PR-5.0, (c) PR-7.5, and (d) PR-10.0
Insets showing the corresponding cross-sectional morphologies

2.2 Effect of phenolic resin content on thermal shock behaviors

Thermal shock tests from 1200 ℃ to room temperature were carried out in static air for 20 cycles, with a cumulative oxidation time of 100 min. The weight loss curves with the thermal shock cycles are illustrated in Fig. 2. The weight losses of all samples increase with the thermal shock test proceeding, initially decreasing and then increasing as the phenolic resin content increases. The PR-7.5 exhibits the lowest weight loss (*i.e.*, 27.17%), which is 35.09%, 18.23%, and 52.23% lower than PR-0, PR-5.0, and PR-10.0, respectively. Notably, PR-10.0 has the highest weight loss despite its compact structure and large thickness.

Fig. S3 shows the macroscopic surface morphologies of PR-0 to PR-10.0 after thermal shock. The phenolic resin affects the mass loss of the samples during thermal shock by influencing the surface defects of the coatings after thermal shock. Figs. 3(a-d) provide the microscopic morphologies of the coatings after thermal shock tests. The phenolic resin-free PR-0 (Fig. 3(a)) exhibits macroscopically spalled oxide layers after 20 thermal cycles (with cumulative oxidation of 100 min), where the interconnected pore formation due to crack propagation exacerbates the mass loss. When the phenolic resin is added into the coating, the relatively continuous oxide scales are formed, as shown in Figs. 3(b-d). However, the porous structure of PR-5.0 retains many surface holes after thermal shock. When 7.5% phenolic resin is introduced into the coating (PR-7.5), noticeable surface hole-healing is observed due to its compact structure and the relatively low resin content. According to the elemental surface analyses shown in Figs. 3(c_1-c_3), this healing phase is identified as ZrO_2-stabilized borosilicate glass. Although PR-10.0 is compact, the excessive phenolic resin contributes to the formation of surficial surface and inner pores due to resin carbonization, carbon oxidation and successive volatilization of carbon oxides during thermal shock.

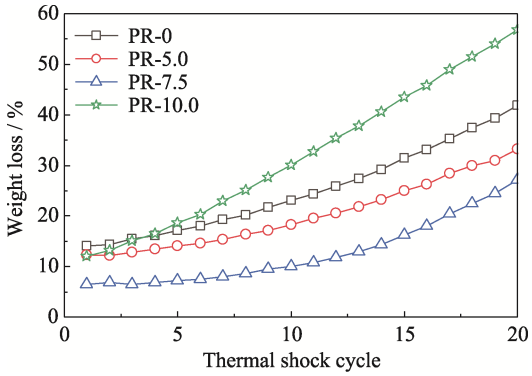

Fig. 2 Weight loss of C/CA with different coatings during thermal shock at 1200 ℃

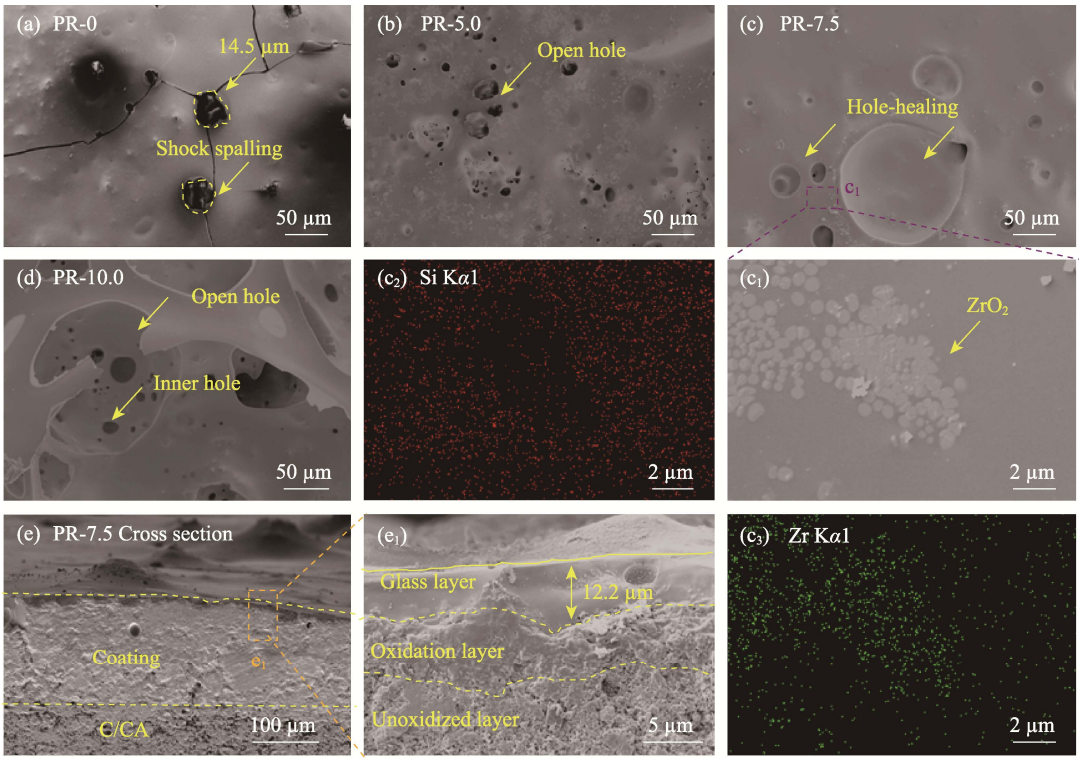

Fig. 3 (a-d) Surface morphologies of PR-0, PR-5.0, PR-7.5, and PR-10.0 after thermal shock; (c_1-c_3) Surface microstructures under high magnification and corresponding elemental analyses; (e, e_1) Cross-sectional morphologies of PR-7.5

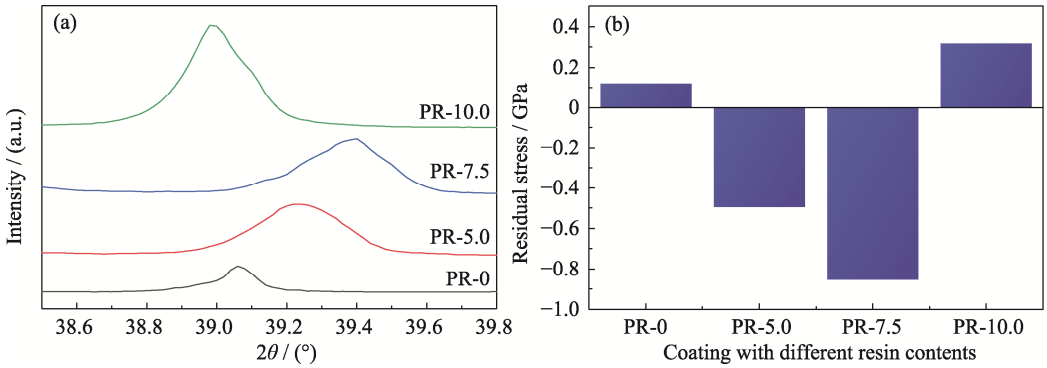

Fig. 4 (a) XRD patterns near 2θ=39° of different coatings, and (b) residual stress of the coating calculated according to the shift of diffraction peaks in (a)

Figs. 3(e, e_1) show the cross-sectional morphologies of PR-7.5 after thermal shock, revealing that the coating closely adheres to the substrate without interfacial debonding or cracking after cyclic thermal shock. As shown in Fig. 3(e_1), the coating can be divided into three layers: a glass layer, an oxidation layer and an unoxidized layer. The bonding between the layers is tight with no interfacial cracks, which verifies the effective oxidation protection provided by the coating.

The surface defects, especially the cracks generated during thermal shock, are influenced by both the original microstructure and healing ability of the formed oxide film, as well as the residual stress of the as-prepared coating[13]. The tensile stress produced by the shrinkage of the coating during the cooling process is one of the main reasons for the formation of cracks. When residual compressive stress is present in the prepared coating, the tensile stress generated during thermal shock is mitigated, thereby preventing cracking, and vice versa. Fig. 4(a) shows the diffraction peak shift of $ZrSi_2$ (131) crystal plane near 2θ=39° in the XRD patterns. With the increase in phenolic resin content, the diffraction peak initially shifts significantly to the right and subsequently shifts to the left, indicating that phenolic resin modifies the residual stress within the coating. Specifically, the $ZrSi_2$ (131) (PDF#72-1272) has

a standard diffraction peak at $2\theta_0$=39.106°, while the corresponding peaks for PR-0 to PR-10.0 are located at 2θ=39.065°, 39.273°, 39.395°, and 38.996°, respectively. Assuming that $ZrSi_2$ particles are isotropic and undergo only elastic deformation, the stress within the $ZrSi_2$ component of the coating can be calculated according to the Bragg equation $n\lambda=2d\sin\theta$ and Hooke's law $\sigma=E\times(\Delta d/d_0)$, where E represents the elastic modulus of $ZrSi_2$ (120.660 GPa), Δd is the change in crystal surface spacing, d and d_0 correspond to the distances between crystal faces in the as-prepared and unstressed states, and σ denotes the residual stress. Fig. 4(b) shows the calculated residual stress of the coatings according to the XRD results. PR-0 has a tensile stress of 0.119 GPa, while compressive stresses in PR-5.0 and PR-7.5 are observed to be 0.496 and 0.853 GPa, respectively. As the phenolic resin content increases to 10.0%, the stress in PR-10.0 reverts to a tensile stress of 0.315 GPa. The compressive stress in PR-7.5 is beneficial for inhibiting the cracking of the coating during thermal shock, thus protecting the C/CA substrate from oxidation[14]. However, PR-10.0 is prone to cracking due to the residual tensile stress during thermal shock, which likely contributes to its relatively high weight loss[15].

Obviously, the phenolic resin content significantly affects the residual stress within the coating, which can be explained in terms of the distribution of the resin and ceramic particles, and the resin shrinkage[16]. In PR-0 coating only containing PVB resin, the resin cannot fully encapsulate the ceramic particles, thereby forming a bonding structure solely among particles. During the curing process, the shrinkage of interparticle bonding resin exerts residual tensile stress on the ceramic particles[17]. When phenolic resin (5.0% and 7.5%) is added to the coating, the resin can fully encapsulate the ceramic particles. During the curing process, the shrinkage of the surrounding resin compresses the ceramic particles, resulting in compressive stress while shifting the diffraction peaks to the right. PR-7.5 with a greater amount of phenolic resin presents a greater residual compressive stress than PR-5.0. However, when the phenolic resin content increases to 10.0%, the coating thickness greatly increases from 173.6 μm to 254.1 μm. The large thickness may result in an unignorably uneven curing of the resin from the surface to the interior. As the resin in the surface layer is completely cured, the curing shrinkage of the resin in the inner layer exerts a tensile force on the surface, resulting in the generation of residual tensile stress in the surface[18].

2.3 Effect of temperature on the oxidation behaviors of PR-7.5

Considering the excellent thermal shock resistance of PR-7.5, an in-depth exploration was conducted to investigate the oxidation behaviors of the coated C/CA within a temperature range of 800–1200 ℃. As shown in Fig. 5, it is obvious that the weight loss of PR-7.5 coated C/CA decreases with the increasing temperature. Specifically, the weight losses are 17.46%, 8.15% and 3.15% after oxidation at 800 ℃ for 100 min, 1000 ℃ for 120 min and 1200 ℃ for 120 min, respectively. In comparison, the uncoated C/CA exhibits a weight loss of 44.60% after oxidation at 800 ℃ for only 20 min. This clearly demonstrates that PR-7.5 significantly enhances the service life of C/CA at 800–1200 ℃.

The total weight loss of the sample encompasses the oxidation-induced weight gain of the ceramic phases, the oxidation-induced weight loss of the C/CA substrate, and the weight loss associated with resin carbonization and oxidation. These factors are significantly influenced by the integrity of the coating and its oxide film present on the surface. Fig. 6 shows the morphologies of PR-7.5 after oxidation at different temperatures. At 800 ℃, notable oxidation of the ceramic particles within the coating occurs, facilitating the formation of a borosilicate glass film, according to the thermogravimetric analysis results in Fig. S4. The oxidation of the ceramics exhibits a slow weight gain due to the relatively low temperature, which is attributed to the formation of B_2O_3 from B_4C[19]. B_2O_3 has a relatively high viscosity, resulting in a discontinuous oxide film on the coating surface, which partially protects the substrate. Additionally, the nanoscale pores and cracks induced by the resin carbonization and oxidation are not adequately healed at this temperature (Fig. 6(a)). These defects provide channels for oxygen to diffuse into C/CA, resulting in a relatively high weight loss of the sample at 800 ℃ (Fig. 5). When the oxidation temperature is elevated to 1000 ℃, the ceramics undergo rapid oxidation to form a continuous borosilicate glass film with self-healing capacity[20]. Specially, SiB_6 and $ZrSi_2$ start to oxidize (Fig. S4), producing excessive ZrO_2 and SiO_2, which improve the stability of the glass film to

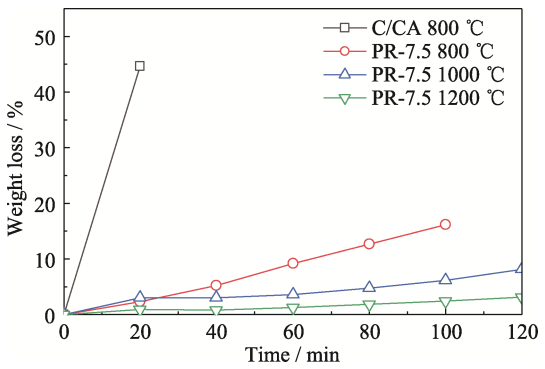

Fig. 5 Weight loss of the C/CA with PR-7.5 during oxidation at 800–1200 ℃

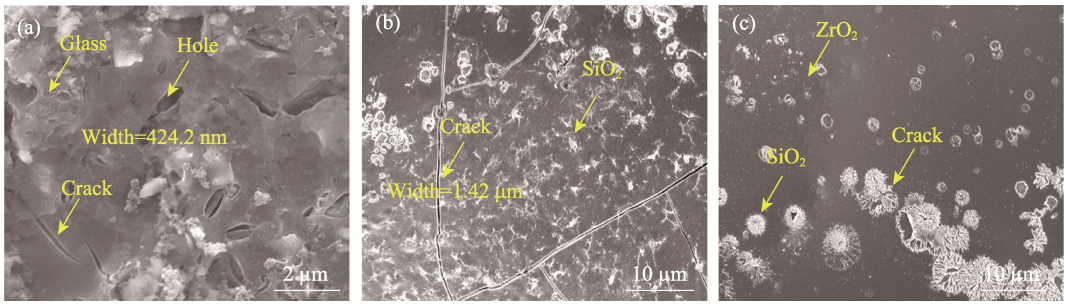

Fig. 6 Surface morphologies of the oxidized PR-7.5 at (a) 800, (b) 1000 and (c) 1200 ℃

prevent the oxygen from diffusing inward (Fig. 6(b)). This leads to a reduction in the oxidation weight loss of the sample at 1000 ℃ (Fig. 5). At 1200 ℃, although B_2O_3 volatilizes more rapidly, leaving SiO_2-rich regions with micro-crack characteristics (Fig. 6(c)), the oxide film remains stable. At this point, part of ZrO_2 integrates into the glass network in the form of a solid solution, forming Si–O–Zr or B–O–Zr bonds to enhance the crosslinking properties of the glass network. The excess ZrO_2 is dispersed in the glass film in the form of nanoparticles to enhance the mechanical properties[21]. Meanwhile, the glass phase, which exhibits excellent fluidity at elevated temperatures, demonstrates strong self-healing capabilities, effectively reducing defects on the coating surface after oxidation. The diminished surface defects and the massive oxidation of ceramics contribute to the lowest oxidation weight loss at 1200 ℃ (Fig. 5).

In addition, the interfacial bonding strength of the C/CA composites protected by PR-7.5 and the retention rate of the bending strength after thermal shock were characterized. As shown in Fig. S5(c), the strengths of the original C/CA and the C/CA with the coating were measured at 7.030 and 6.840 MPa, respectively. In Figs. S5(a, b), fracture occurs in the C/CA substrate, indicating that the interfacial bonding strength is comparable to the tensile fracture strength of the substrate. Similarly, the C/CA protected by PR-7.5 has a bending strength of 15.650 MPa after oxidation at 1200 ℃, with a retention rate of the bending strength exceeding 90%. This demonstrates that PR-7.5 can effectively protect the C/CA substrate from significant damage caused by oxidation. Furthermore, oxidation weight loss measurements of three additional sample groups were systematically performed (Fig. S6), followed by oxidation kinetics modeling using the experimental data. The derived fitting coefficients are presented in Table S1. Through parametric analysis of these fitting results, the oxidation activation energy was quantitatively determined as graphically presented in Fig. S7. Remarkably, the PR-7.5 coating exhibits a negative activation energy of –39.86 kJ/mol, thermodynamically confirming its exceptional oxidation resistance with the lowest oxidative degradation tendency among all investigated systems.

Herein, a temperature-dependent anti-oxidation mechanism for the coating system is proposed, wherein the total oxidation mass loss of the specimen is synergistically governed by the competitive interaction between dynamic healing capacity of oxide films and defect evolution. At 800 ℃, the relatively high viscosity of glass film combined with ineffective healing of nanopores and microcracks generated from resin carbonization/oxidation, contributes to slightly elevated oxidation weight loss. When the temperature increases to 1000 ℃, inward diffusion of oxygen is suppressed by the continuous borosilicate glass film formed on specimen surface, thereby leading to a reduced weight loss. However, residual unhealed surface cracks persist, thus limiting the optimal anti-oxidation performance. At 1200 ℃, the volumetric expansion induced by rapid oxidation of ceramic phases, along with the ZrO_2 pinning phase formed through $ZrSi_2$ conversion, synergistically maintains the structural stability of the oxide layer. Simultaneously, the significantly enhanced flow-induced self-healing capability of the glass phase results in minimal surface defects and the lowest oxidation weight loss observed in the specimen. In general, the PR-7.5 demonstrates superior oxidation resistance at 800–1200 ℃ compared with other coatings, attributed to its dense structure, which can rapidly form a continuous glass layer during the initial stage of oxidation, and its high residual compressive stress, which effectively prevents crack initiation and propagation.

3 Conclusions

In a word, a structurally dense ceramic-resin composite coating with robust interfacial bonding was fabricated on the C/CA substrate at ambient temperature. Concurrently, the residual compressive stress (0.853 GPa) induced by resin curing shrinkage in the PR-7.5 coating significantly enhanced its densification, effectively suppressing crack initiation and propagation during

thermal shock from 1200 ℃ to room temperature. After undergoing 20 thermal cycling tests in static air, PR-7.5 exhibited the optimal oxidation-protective performance, achieving a weight loss rate of 27.17%, which was 35.09%, 18.23%, and 52.23% lower than those of PR-0, PR-5.0, and PR-10.0, respectively. Systematic investigations revealed the oxidation resistance mechanism of the coating in the medium temperature range (800–1200 ℃). The volumetric expansion resulting from ceramic oxidation, along with the healing of the glass phase, synergistically compensated for structural defects caused by resin pyrolysis, thereby dynamically maintaining the coating's structural integrity. Specifically, the weight losses under exposure to 800 ℃/100 min, 1000 ℃/120 min, and 1200 ℃/120 min conditions were 17.46%, 8.15%, and 3.15%, respectively, markedly extending the high-temperature service life of C/CA compared to the uncoated samples. This work breaks the limitations of conventional high-temperature sintering processes and establishes a room-temperature film-forming technology, thereby providing a cost-effective anti-oxidation solution for C/CA composites. Through tailoring ceramic component gradients and microstructure design, the protective capabilities of the coating can be extended to other temperature regimes.

Supporting Materials

Supporting materials related to this article can be found at https://doi.org/10.15541/jim20250103.

References:

[1] LEVENTIS N, SOTIRIOU-LEVENTIS C, ZHANG G, *et al*. Nanoengineering strong silica aerogels. *Nano Lett.*, 2002, **2:** 957.

[2] PIERRE A C, PAJONK G M. Chemistry of aerogels and their applications. *Chem. Rev.*, 2002, **102:** 4243.

[3] ZHANG W, HU C, LI J, *et al.* Insight into the origin of oxidation behaviors of carbon fiber reinforced carbon aerogel composites with different porous skeletons. *Carbon*, 2023, **209:** 118008.

[4] YANG D, DONG S, HONG C, *et al*. Preparation, modification, and coating for carbon-bonded carbon fiber composites: a review. *Ceram. Int.*, 2022, **48:** 14935.

[5] ZHANG S, MA Y, SURESH L, *et al*. Carbon nanotube reinforced strong carbon matrix composites. *ACS Nano*, 2020, **14:** 9282.

[6] YAN M, HU C, LI J, *et al*. An unusual carbon-ceramic composite with gradients in composition and porosity delivering outstanding thermal protection performance up to 1900 ℃. *Adv. Funct. Mater.*, 2022, **32:** 2204133.

[7] YAN M, HU C, LI J, *et al*. Construction of a ceramic coating with low residual stress on C/CA composites for thermal protection at ultra-high temperatures. *Compos. B Eng.*, 2023, **266:** 110970.

[8] XU L, LI X, NI L, *et al*. Ablation behavior of functional gradient ceramic coating for porous carbon-bonded carbon fiber composites. *Corros. Sci.*, 2018, **142:** 145.

[9] LI X, FENG J, WU X, *et al*. Ablation resistance of C/C-SiCO nanoporous ceramic composites with $TaSi_2$-$MoSi_2$-ZrB_2-borosilicate glass coating. *Process. Appl. Ceram.*, 2023, **17:** 384.

[10] XU B, AN Y, WANG P, *et al*. Microstructure and ablation behavior of double anti-oxidation protection for carbon-bonded carbon fiber composites. *Ceram. Int.*, 2017, **43:** 783.

[11] MA J, LI J, GUO P, *et al.* Tailoring microstructures of carbon fiber reinforced carbon aerogel-like matrix composites by carbonization to modulate their mechanical properties and thermal conductivities. *Carbon*, 2022, **196:** 807.

[12] LI J, GUO P, HU C, *et al*. Fabrication of large aerogel-like carbon/carbon composites with excellent load-bearing capacity and thermal-insulating performance at 1800 ℃. *ACS Nano*, 2022, **16:** 6565.

[13] CHEN Z, CUI X, WANG X, *et al*. Novel high-entropy $(La_{0.35}Gd_{0.35}Y_{0.35}Sm_{0.35}Yb_{0.6})Zr_2O_7$ thermal barrier coatings: thermal cycling performance and failure behavior. *Ceram. Int.*, 2024, **50(24):** 54716.

[14] GABB T P, ROGERS R B, NESBITT J A, *et al.* Influences of processing and fatigue cycling on residual stresses in a NiCrY-coated powder metallurgy disk superalloy. *J. Mater. Eng. Perform.*, 2017, **26:** 5237.

[15] TAO S, YANG J, SHAO F, *et al.* Atmospheric plasma sprayed thick thermal barrier coatings: microstructure, thermal shock behaviors and failure mechanism. *Eng. Fail. Anal.*, 2022, **131:** 105819.

[16] DEWANGAN B, CHAKLADAR N D. Modelling of residual stress during curing of a polymer under autoclave conditions and experimental validation. *Comput. Mater. Sci.*, 2024, **241:** 113038.

[17] O'MASTA M R, BUI P P, LARSON N M, *et al.* Reinforcement induced microcracking during the conversion of polymer-derived ceramics. *Acta Mater.*, 2024, **275:** 120053.

[18] VAZ R F, GARFIAS A, ALBALADEJO V, *et al.* How increasing cold spray coatings thickness affects their residual stress and properties. *Surf. Coat. Technol.*, 2024, **485:** 130867.

[19] LIU P, ZHANG X, XUE Y, *et al*. A novel B_2O_3/B_4C-modified composite adhesive with wide operative temperature range for alumina fiber fabric bonding. *Ceram. Int.*, 2021, **47:** 6643.

[20] ZHU S, XU Y, LIU R, *et al.* Preparation of high-temperature antioxidant coatings on tantalum-based surfaces by atmospheric plasma spraying and their microstructural characterization. *Surf. Coat. Technol.*, 2025, **501:** 131928.

[21] CONNELLY A J, TRAVIS K P, HAND R J, *et al.* Composition-structure relationships in simplified nuclear waste glasses: 2. The effect of ZrO_2 additions. *J. Am. Ceram. Soc.*, 2011, **94:** 137.

C/CA 表面陶瓷-树脂涂层的简易制备与中温抗氧化性能

田洪旺[1,2], 罗龙飞[3], 胡成龙[1], 闫 猛[1], 庞生洋[1], 李 建[1], 汤素芳[1]

(1. 中国科学院 金属研究所, 沈阳 110016; 2. 中国科学技术大学 材料科学与工程学院, 沈阳 110016; 3. 西安航天复合材料研究所, 西安 710025)

摘 要: 碳纤维增强碳气凝胶(C/CA)复合材料是同时满足隔热和承载应用需求的最具潜力的候选材料之一。在 C/CA 上制备抗氧化涂层用于解决其易氧化问题, 是促进其在氧化环境中应用的重要方法。然而, 目前已报道的 C/CA 抗氧化涂层主要用于提升材料的烧蚀性能, 且涂层制备工艺常涉及高温热处理过程, 这会导致 C/CA 热导率增加, 进而降低隔热效果。本研究在室温下采用简单的浆料刷涂-干燥方法, 在 C/CA 上制备了一系列陶瓷-树脂涂层, 并研究了酚醛树脂含量对涂层结构、残余应力、热冲击以及氧化行为的影响。结果表明, 得益于树脂的黏接作用和固化收缩作用, PR-7.5 涂层(料浆中酚醛树脂质量分数为 7.5%)结合强度与基底本征断裂强度相近, 且具有 0.853 GPa 的残余压应力, 显著提升了其热震性能; 而进一步提高树脂含量(PR-10.0, 料浆中酚醛树脂质量分数为 10.0%), 涂层因树脂不均匀固化导致收缩不一致而产生了残余拉应力, 热震时易开裂。实验结果显示, PR-7.5 在 800 ℃下氧化 100 min、1000 ℃下氧化 120 min 以及 1200 ℃下氧化 120 min 后失重率分别为 17.46%、8.15%和 3.15%; 而没有涂层的 C/CA 复合材料在 800 ℃下氧化 20 min 后失重率高达 44.60%。本工作为提高 C/CA 的抗氧化性能提供了一种全新且简单的途径, 拓展了其在温和氧化环境中的应用。

关 键 词: C/CA 复合材料; 涂层; 氧化; 残余应力; 界面结合

中图分类号: TQ174 **文献标志码:** A **文章编号:** 1000-324X(2026)03-0401-08

Supporting Materials

Facile Fabrication of Ceramic-resin Coatings on C/CA Composites for Oxidation Protection at Medium Temperatures

TIAN Hongwang[1,2], LUO Longfei[3], HU Chenglong[1], YAN Meng[1],
PANG Shengyang[1], LI Jian[1], TANG Sufang[1]

(1. Institute of Metal Research, Chinese Academy of Sciences, Shenyang 110016, China; 2. School of Materials Science and Engineering, University of Science and Technology of China, Shenyang 110016, China; 3. Xi'an Aerospace Composites Research Institute, Xi'an 710025, China)

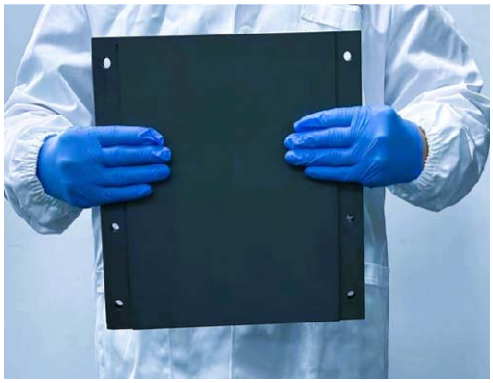

Fig. S1 Macrophotograph of the coated C/CA panel with a size of 300 mm×300 mm×25 mm

Fig. S2 presents the XRD patterns of C/CA with and without coatings. The results show all of coatings have the same diffraction peaks of SiC, B_4C, $ZrSi_2$ and SiO_2. Additionally, the B_2O_3 and SiB_6 phases are not detected due to the relatively low contents. Differently, because PR-0 is thin and has many large pores, the characteristic peak of amorphous CA can be detected in the 2θ range of 20°–28°. However, the amorphous diffraction peak disappears in PR-5.0 because of the increasing coating thickness and compactness. In PR-7.5 and PR-10.0, the amorphous diffraction peaks appear again in the 2θ range of 18°–25°, which are originated from the phenolic resin,

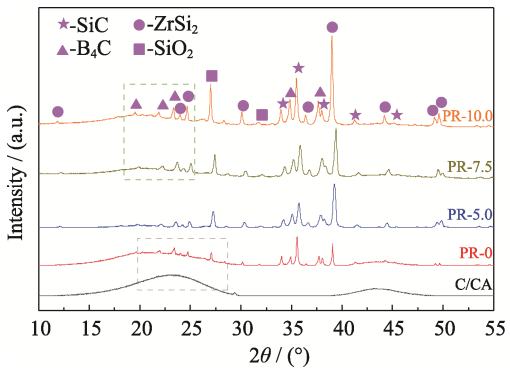

Fig. S2 XRD patterns of C/CA without and with different coatings

and their intensities show an upward trend with the increasing phenolic resin contents. The result is in correspondence with the aggregation of phenolic resin manifested on the surface morphology as shown in Fig. 1(d).

Fig. S3 presents the macroscopic surface morphologies of PR-0 to PR-10.0 after thermal shock. PR-0 exhibits pronounced thermal spalling with crack widths exceeding 10 μm (Fig. S3(a)), which can be attributed to the original large pores hindering the formation of a dense oxide layer. As the resin content increases, PR-5.0 and PR-7.5 demonstrate progressively reduced surface defects with complete elimination of macroscopic cracks (Figs. S3(b, c)). However, further augmentation of resin in PR-10.0 results in many pores and cracks that are difficult to heal, with a width of more than 30 μm (Fig. S3(d)) since the defects can be generated by resin pyrolysis and insufficient filler by ceramic-derived glassy phases.

Fig. S4 shows the initial oxidation temperatures of each ceramic phase using TG. The results show that B_4C can rapidly oxidize to produce B_2O_3 at 600–700 ℃, and SiB_6 can rapidly oxidize to form B_2O_3 and SiO_2 at 900–1000 ℃. $ZrSi_2$ can be oxidized to form SiO_2 and

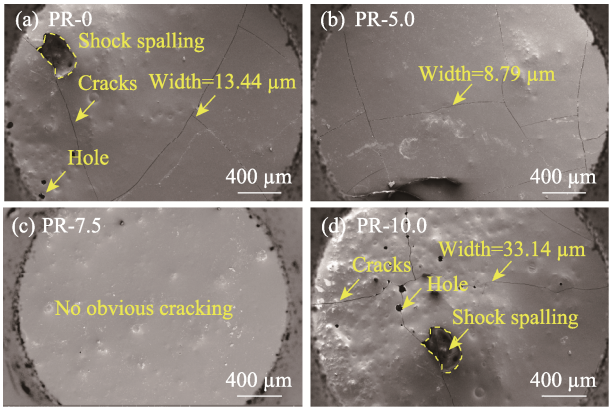

Fig. S3 Macroscopic surface morphologies of the different coatings after thermal shock from 1200 ℃ to room temperature (a) PR-0; (b) PR-5.0; (c) PR-7.5; (d) PR-10.0

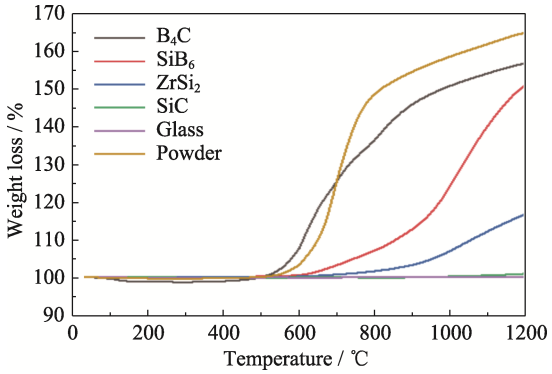

Fig. S4 Thermogravimetric analyses of ceramics in the coating

ZrO_2 at 1200 ℃. SiC oxidizes slowly below 1200 ℃. The "powder" composed of the above-mentioned ceramics can rapidly oxidize below 800 ℃, and the "glass" composed of the SiO_2 and B_2O_3 products remains stable below 1200 ℃, meeting the service requirements of the coating at 800–1200 ℃. In this work, ceramic particles with different initial oxidation temperatures were selected to form the ceramic phase in the coating, so that the coating had ceramic phases for oxidation and expansion at different temperatures, achieving a stepped-type cooperative protection. Meanwhile, ZrO_2 and SiC were selected as binding particles to ensure the stable existence of the oxide film at high temperatures. The specific oxidation reactions involved are as follows:

$$ZrSi_2 + 3O_2 = ZrO_2 + 2SiO_2 \quad (S1)$$

$$SiB_6 + 5.5O_2 = SiO_2 + 3B_2O_3 \quad (S2)$$

$$SiC + 2O_2 = SiO_2 + CO_2 \quad (S3)$$

$$B_4C + 4O_2 = 2B_2O_3 + CO_2 \quad (S4)$$

$$SiO_2 + B_2O_3 = SiO_2 \cdot B_2O_3 \quad (S5)$$

The interfacial bonding strength and the retention rate of the bending strength of the coated C/CA composites were also investigated before and after thermal shock. The interfacial bonding strength between the coating and the substrate was measured by a tensile test and the fracture morphologies are shown in Figs. S5(a, b). The fracture occurs in the C/CA substrate rather than at the interface, indicating that the interfacial bonding strength is comparable to the tensile fracture strength of the substrate. As shown in Fig. S5(c), strength of the original C/CA and coated C/CA are close to 7.030 and 6.840 MPa, respectively, attributed to the good adhesive ability of the resin. Similarly, the coated sample shows a high bending strength of 15.650 MPa with a retention rate of 90.20% after thermal shock. This demonstrates that the C/CA substrate is well protected by PR-7.5 without significant oxidation-induced damage.

In Table S1, the parameters a and b of the linear equation are fitted using the data in Fig. S6. Then, k and ln$k$ are calculated from a. The linear correlation coefficient R^2 of the fitted straight line is mostly above 0.9, which indicates that the linear fitting goodness of the oxidation weight loss data of the samples is high. Finally, based on the relationship between ln$k$ and $1/T$, the variation of the oxidation activation energy (E_a) of the four groups of coatings with the reciprocal of temperature was fitted, and the results are shown in Fig. S7.

The details are as follows:

$$w = at + b \quad (S6)$$

In which, w is the weight loss, a (min^{-1}) and b are the linear fitting parameters, and t is the oxidation time. Differentiate both sides of the linear fitting formula with respect to t.

$$dw = kdt \quad (S7)$$

k (s^{-1}) is the constant of weight loss, and $k=a/60$. The relationship between k and temperature can be expressed using the Arrhenius equation:

$$k = A\exp\left(-\frac{E_a}{RT}\right) \quad (S8)$$

Take the natural logarithm (logarithm with base e) of both sides of the equation.

$$\ln k = \ln A - \frac{E_a}{RT} \quad (S9)$$

Where A refers to the pre-exponential factor, E_a represents the apparent activation energy, T is the absolute temperature, and R=8.314 J/(mol·K).

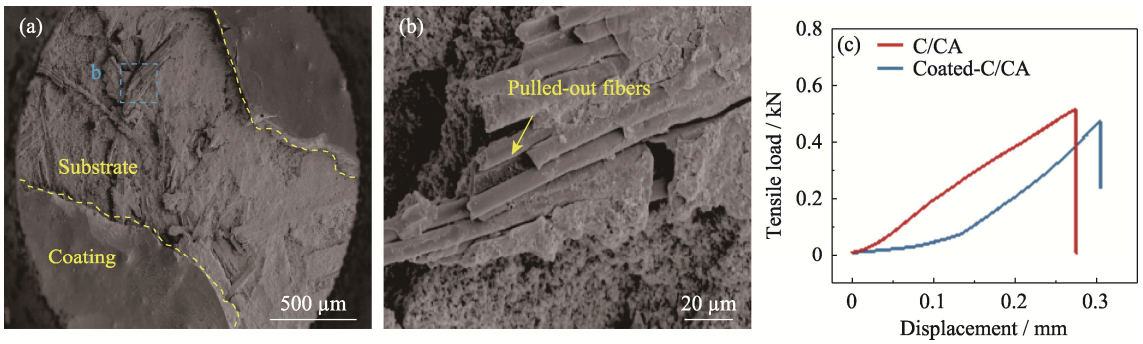

Fig. S5 (a, b) Surface morphologies of the sample after the tensile test, and (c) tensile curves of the C/CA substrate and the coated C/CA

Table S1 Fitting results of oxidation kinetics equation parameters of PR-0, PR-5.0, PR-7.5, and PR-10.0 at 800, 1000 and 1200 ℃

Temperature/℃	Sample	a/(×10^{-2}, min^{-1})	b	R^2	k/(×10^{-3}, s^{-1})	ln$k$
800	PR-0	43.45	–4.305	0.9974	7.2417	–4.9279
	PR-5.0	35.9	8.9301	0.9996	5.9833	–5.1188
	PR-7.5	17.42	–1.3518	0.9974	2.9033	–5.8419
	PR-10.0	40.84	8.8932	0.9948	6.8067	–4.9899
1000	PR-0	66.32	–4.2528	0.9999	11.0533	–4.5050
	PR-5.0	8.75	0.9611	0.9611	1.4583	–6.5305
	PR-7.5	5.15	0.8934	0.8934	0.8583	–7.0605
	PR-10.0	18.68	5.5384	0.9951	3.1133	–5.7721
1200	PR-0	81.66	–9.239	0.9996	13.61	–4.2970
	PR-5.0	10.72	6.0556	0.8625	1.7867	–6.3274
	PR-7.5	2.37	0.0858	0.9112	0.395	–7.8366
	PR-10.0	35.01	3.0509	0.9928	5.835	–5.1439

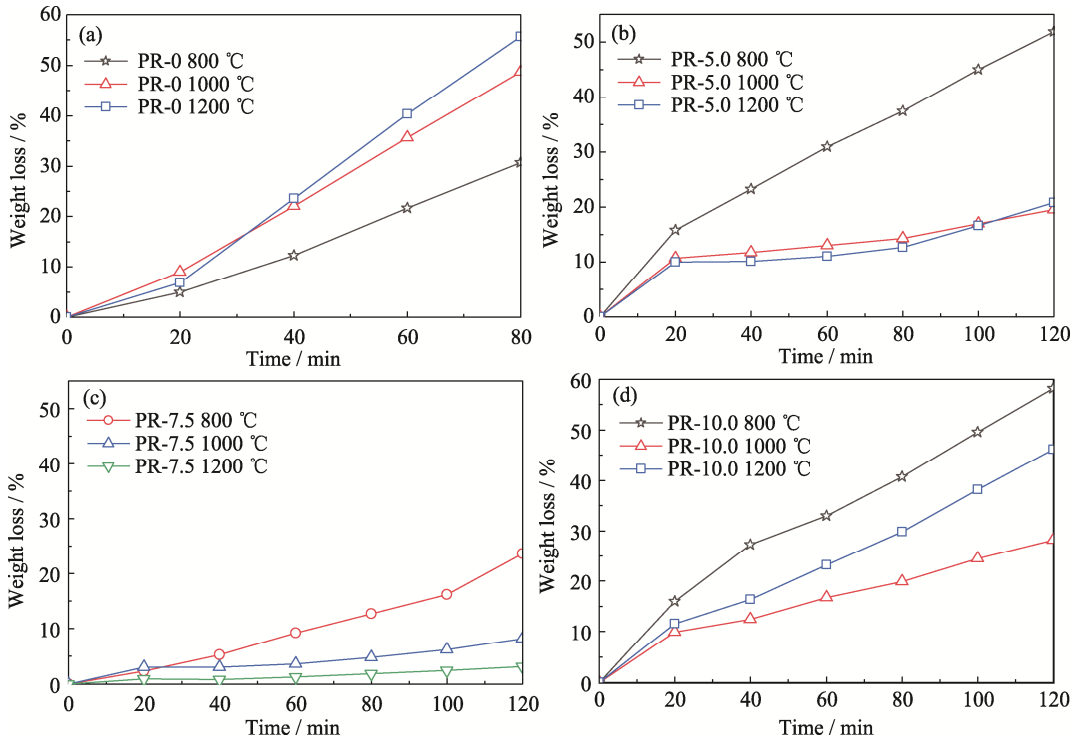

Fig. S6 Weight loss of the C/CA with different coatings under oxidation tests in the temperature range of 800–1200 ℃
(a) PR-0; (b) PR-5.0; (c) PR-7.5; (d) PR-10.0

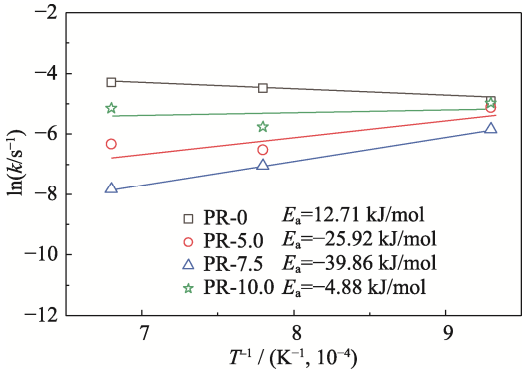

Fig. S7 Oxidation rate curves with 1/T for the different coated C/CA

The Arrhenius curves of oxidation rates for C/CA with different coatings are depicted in Fig. S7. The relationship between ln$k$ and 1/T is almost linear, and the oxidation activation energy can be calculated from the slope. The activation energies of PR-0, PR-5.0, PR-7.5, and PR-10.0 are 12.71, –25.92, –39.86, and –4.88 kJ/mol, respectively. The absolute value of oxidation activation energy represents the oxidation-resistant ability of the coatings. The remarkably low value of PR-7.5 verifies its superior antioxidant performance. Since the oxidation rates decrease with the rising temperature for the coating with phenolic resin, the calculated activation energy values are negative. It is reasonable to deduce that the

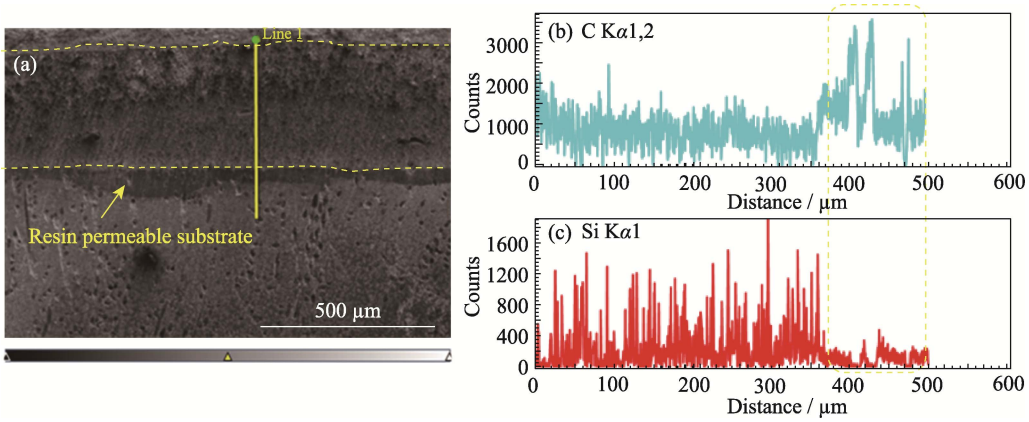

Fig. S8 (a) Cross-sectional microstructure of PR-7.5 and (b, c) elemental line scanning of C and Si in (a)

defects are self-healed effectively at higher temperatures for these coatings.

SEM image (Fig. S8) shows that there is a strip-shaped region with a deep contrast on the side close to the substrate at the interface between the coating and substrate. An elemental line scanning analysis is conducted from the coating towards the substrate, and the results show that the C peak in this region is extremely higher than that in the C/CA substrate (Figs. S8(a, b)). This suggests resin infiltration from the slurry into the substrate during the coating fabrication, followed by resin accumulation near the C/CA surface layer during curing shrinkage. Beyond the adhesive effect of the resin itself, this microstructure creates strong bonding between the ceramic-resin coating and the substrate, resulting in an interfacial strength comparable to that of the substrate.

Testing process of mechanical properties

Bending strength of the original C/CA before oxidation and the C/CA with coating after oxidation (with dimensions of 60 mm×10 mm×5 mm) was tested using the three-point bending method. The span was 50 mm and the loading rate was 2 mm/min. Bending strength calculation formula $\sigma_b=3PL/2zh^2$. Among them, P is the breaking load (N), L is the span (mm), z is the width of the sample (mm), and h is the thickness of the sample (mm).

According to the measurements, the C/CA protected by PR-7.5 has a bending strength of 15.650 MPa after oxidation at 1200 ℃, with a strength retention rate exceeding 90%. This is attributed to the formation of a continuous and dense glass film on the coating surface during oxidation, which acts as an effective barrier against oxygen infiltration, thereby mitigating oxidative degradation of the C/CA substrate.

The interfacial bonding strength of the coating was determined by tensile tests, and the test method was in accordance with the American Society for Testing and Materials standard ASTMC633-79. The sample with size of 20 mm (length)×15 mm (width)×10 mm (height) was adhered to the upper and lower fixtures by epoxy resin adhesive with circular bonding area in 9 mm diameter. Then they were installed on the mechanical testing machine and pulled to fracture with a loading rate of 0.5 mm/min. The formula for the tensile bonding strength of the coating is $\sigma=F_{max}/S$. Among them, F_{max} (N) represents the maximum tensile force during the coating stretching process, and S is the contact area between the coating and the fixture. The final strength values were determined after at least 3 measurements.

According to the measurements, the strength of the original C/CA and the coated C/CA are 7.030 and 6.840 MPa, respectively. The bonding strength of the ceramic-resin coating is comparable to the intrinsic strength of C/CA.